Supplementary Information

Structural insight into the stereoselectivity of *R*-selective nitrilase: Reshaping substrate pocket with an "Extend-and-Lock" strategy for efficient Brivaracetam precursor synthesis

Zhe-Ming Wu[a,b,c], Xi-Peng Li[c], Qian-Nan Wu[c], Yu Lu[c], Chen-Han Zhuang[d], Lin-Jie Zhang[c], Hong-Juan Diao[a,b,c], Ren-Chao Zheng[*a,b,c], and Yu-Guo Zheng[a,b,c]

[a]State Key Laboratory of Green Chemical Synthesis and Conversion, Zhejiang University of Technology, Hangzhou, 310014, China

[b]Engineering Research Center of Bioconversion and Biopurification of Ministry of Education, Zhejiang University of Technology, Hangzhou, 310014, China

[c]Zhejiang Key Laboratory of Bioorganic Synthesis, College of Biotechnology and Bioengineering, Zhejiang University of Technology, Hangzhou, 310014, China

[d]Zhejiang Apeloa Jiayuan Pharmaceutical Co., Ltd., Dongyang, 322118, China

Supporting information for this article is given via a link at the end of the document.

***Corresponding author**:

Prof. Ren-Chao Zheng

College of Biotechnology and Bioengineering

Zhejiang University of Technology

18 Chaowang Road, Hangzhou 310014, China

E-mail: zhengrc@zjut.edu.cn

Table of Contents

Table S1. Primes used in this study.

Amino acid sites	Primers (5'→3')
A55	F: CCCGTATTTC**NNK**GCAGTTCAGACTGGT
	R: TCTGAACTGC**MNN**GAAATACGGGTAGTA
A56	F: CGTATTTCGCT**NNK**GTTCAGACTGGTATCGA
	R: CCAGTCTGAAC**MNN**AGCGAAATACGGGTAGT
T133	F: ACCCCA**NNK**CACTTCGAACGTATGATTT
	R: ACGTTCGAAGTG**MNN**TGGGGTGATAAA
F135	F: ACCCCAACTCAC**NNK**GAACGTATGATTTGGGGT
	R: CATACGTTC**MNN**GTGAGTTGGGGTGATTTTACG
F192	F: CCGGGCAGCGCT**NNK**GGCGAAGGTTTTGCGCAG
	R: AAAACCTTCGCC**MNN**AGCGCTGCCCGGATACAT
F164	F: CTGGCGTGT**NNK**GAACATAACAACCCAC
	R: GTTATGTTCGAA**MNN**CGCCAGCTGACCA
R199	F: GGTTTTGCGCAG**NNK**ATGGAAATCAACATTCGTCAG
	R: GATTTCCAT**MNN**CTGCGCAAAACCTTCGCCAAA
Q58	F: TATTTCGCTGCAGTT**NNK**GACGGTATCG
	R: CAGCTCGATACCGTC**MNN**AACTGCAGCG
T59	F: GCTGCAGTTCAG**NNK**GGTATCGAGCTGCTG
	R: TCAGCAGCTCGATACC**MNN**CTGAACTGCAG
G60	F: GCTGCAGTTCAGGAC**NNK**ATCGAGCTGC
	R: GCTCAGCAGCTCGAT**MNN**GTCCTGAACT
I61	F: GCAGTTCAGGACGGT**NNK**GAGCTGCTGAG
	R: ACCGCTCAGCAGCTC**MNN**ACCGTCCTGA
E62	F: GTTCAGGACGGTATC**NNK**CTGCTGAGCG
	R: GGAACCGCTCAGCAG**MNN**GATACCGTCC
L63	F: CAGGACGGTATCGAG**NNK**CTGAGCGGTT
	R: TTCGGAACCGCTCAG**MNN**CTCGATACCG
L64	F: GACGGTATCGAGCTG**NNK**AGCGGTTCCG
	R: GTGTTCGGAACCGCT**MNN**CAGCTCGATA
S65	F: GGTATCGAGCTGCTG**NNK**GGTTCCGAAC
	R: CAGGTGTTCGGAACC**MNN**CAGCAGCTCG
K281	F: ACAGATCGATCGTCGT**NNK**ATGCTGATGGA
	R: CAGCGTCCATCAGCAT**MNN**ACGACGATCGA
M282	F: ATCGATCGTCGTAAA**NNK**CTGATGGACG
	R: GGCAGCGTCCATCAG**MNN**TTTACGACGA
L283	F: GATCGTCGTAAAATG**NNK**ATGGACGCTG
	R: ACCGGCAGCGTCCAT**MNN**CATTTTACGA
M284	F: CGTCGTAAAATGCTG**NNK**GACGCTGCCGG
	R: ATGACCGGCAGCGTC**MNN**CAGCATTTTAC

Table S2. Screened nitrilases in this work.

Nitrilases	Source	Accession	Stereoselectivity	*E*
***Af*NIT-1**	*Alcaligenes faecalis*	WP_236780549.1	*R*	3.8
***At*NIT**	*Arabidopsis thaliana*	CAD5324840.1	*R*	3.7
***Bn*NIT**	*Brassica napus*	J4E87_006048	*S*	4.6
***Os*NIT**	*Oryza sativa*	NC_029258.1	Nd	Nd
***Br*NIT**	*Brassica rapa*	BAG72074.1	*R*	4.5
***Es*NIT**	*Eutrema salsugineum*	NW_006256829.1	*R*	6.0
***Aa*NIT**	*Arabis alpina*	KFK44999	*R*	4.4
***Kp*NIT**	*Klebsiella pneumoniae*	P10045.1	Nd	Nd
***Rz*NIT**	*Rhodococcus zopfii*	WP_138999863	*R*	3.4
***Gp*NIT**	*Geobacillus pallidus*	ABH04285	Nd	Nd
***Ap*NIT**	*Arthrobacter pascens*	BAJ17399	*R*	1.2
***Af*NIT-2**	*Acidovorax facilis*	WP_236780549.1	Nd	Nd
***Pg*NIT**	*Paraburkholderia graminis*	QCT24552.1	*R*	15
***Ba*NIT$_{M2}$**	*Chimera*	/	*S*	84
***Ps*NIT**	*Pseudomonas*	WP_153649688.1	Nd	Nd
***Rr*NIT**	*Rhodococcus rhodochrous K22*	BAA02127	*S*	5.3
***Bj*NIT**	*Bradyrhizobium japonicum*	HXT67_RS08040	*S*	2.4

Nd= Not detected.

Table S3. The calculated binding free energy (ΔΔGbind) based on MM/PBSA method.

Potential site	E45	Y51	A55	A56	K129	T133
ΔΔG$_{bind}$	-1.628	2.209	-3.254	1.591	4.424	-3.986
Potential site	F135	E136	C163	F164	Y187	P188
ΔΔG$_{bind}$	-4.424	4.648	1.036	2.629	-0.425	-0.651
Potential site	F192	F196	R199	M200		
ΔΔG$_{bind}$	7.546	4.361	6.339	0.232		

Based on MD trajectories, the difference in MMPBSA energy decomposition between WT and (*R*)-/(*S*)-**1a** is defined as $\Delta\Delta G_{bind} = \Delta G_{bind}$ (*R*) - ΔG_{bind} (*S*).

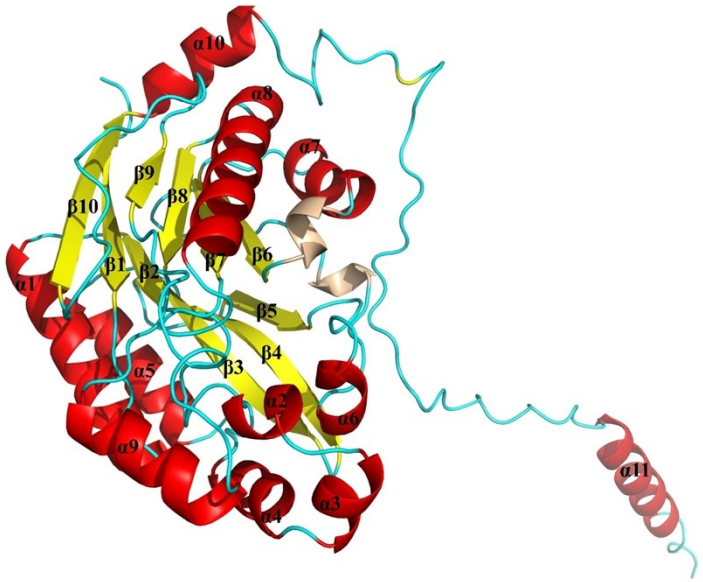

Figure S1. Cartoon diagram of the WT monomer structure. The α-helices are presented in red, while the β-strands are presented in yellow.

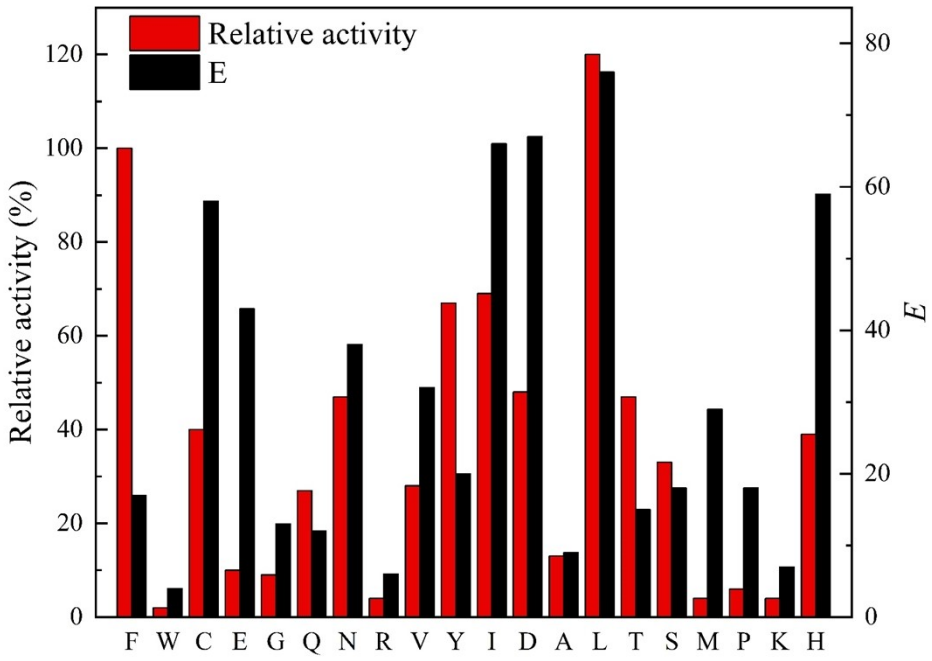

Figure S2. Results of saturation mutagenesis at position 135. The relative activities are shown in red, and the *E* values are shown in black.

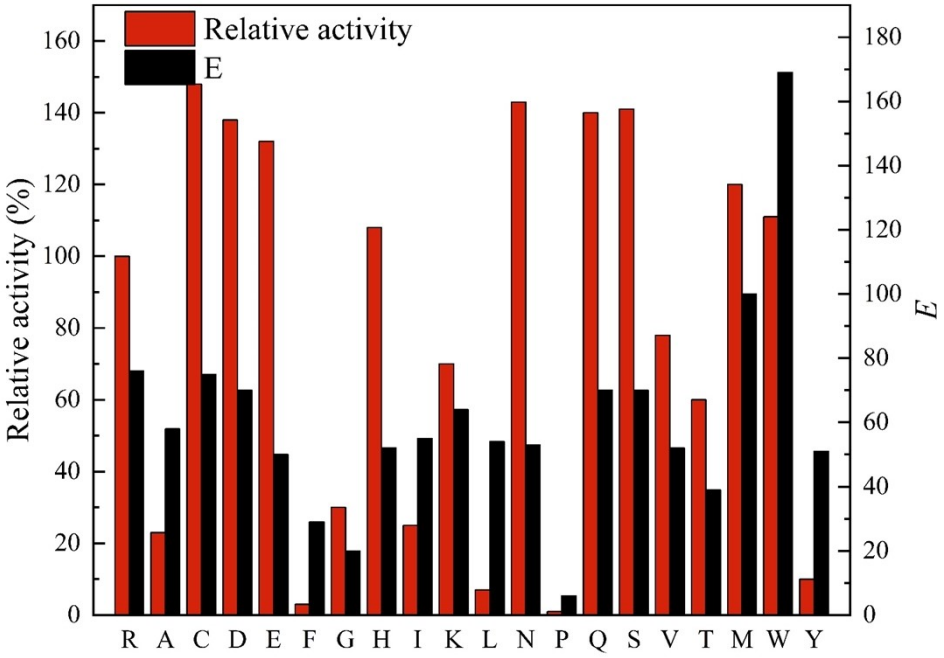

Figure S3. Results of saturation mutagenesis at position 199. The relative activities are shown in red, and the *E* values are shown in black.

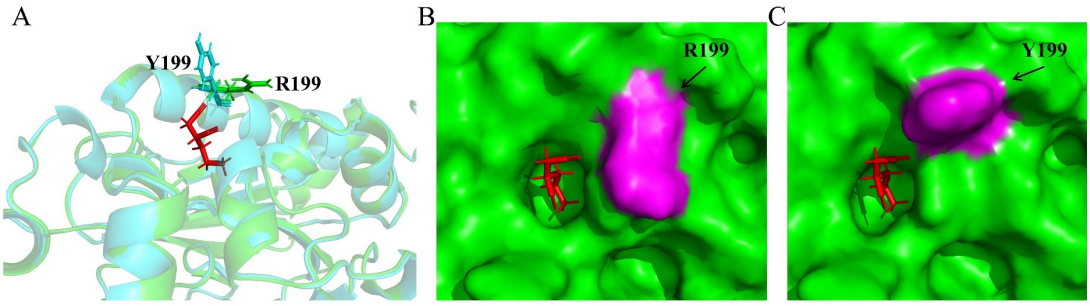

Figure S4. Comparison of steric hindrance conferred by residues R199 and Y199. (A) Structural superposition of R199 and Y199. (B) Surface representation of the steric effect exerted by R199 on the substrate. (C) Surface representation of the steric effect exerted by Y199 on the substrate. The substrates are represented as red stick models.

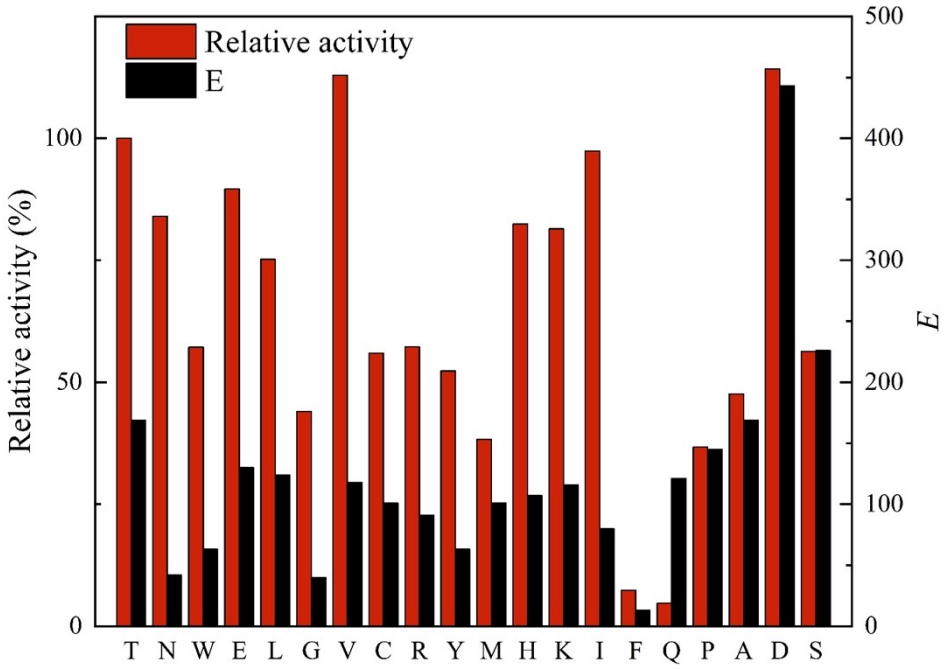

Figure S5. Results of saturation mutagenesis at position 59. The relative activities are shown in red, and the *E* values are shown in black.

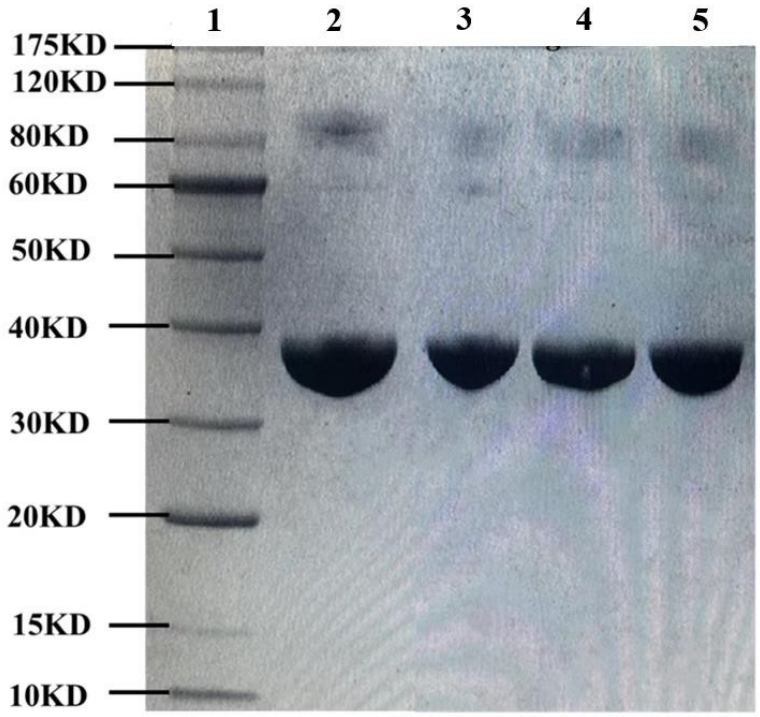

Figure S6. SDS-PAGE analysis of the *Pg*NIT and its variants. Lane 1, the protein molecular weight maker; lane 2: *Pg*NIT; lane 3: F135L; lane 4：F135L/R199W; lane 5: T59D/F135L/R199W.

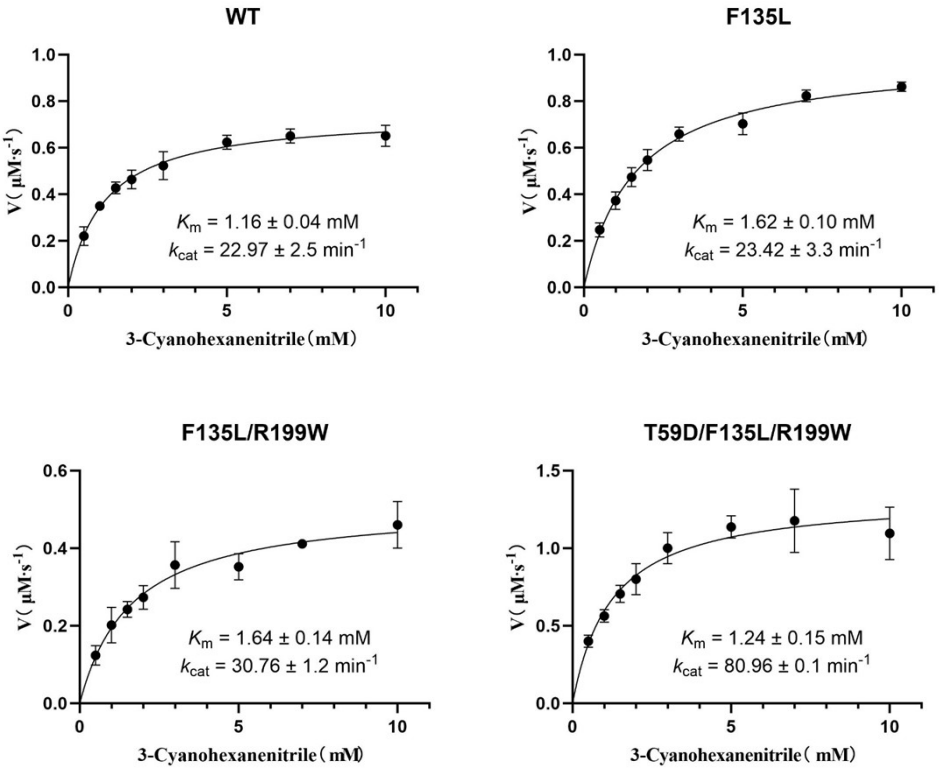

Figure S7. Michaelis-Menten kinetics of wild-type *Pg*NIT (WT) and its mutants towards substrate **1a**.

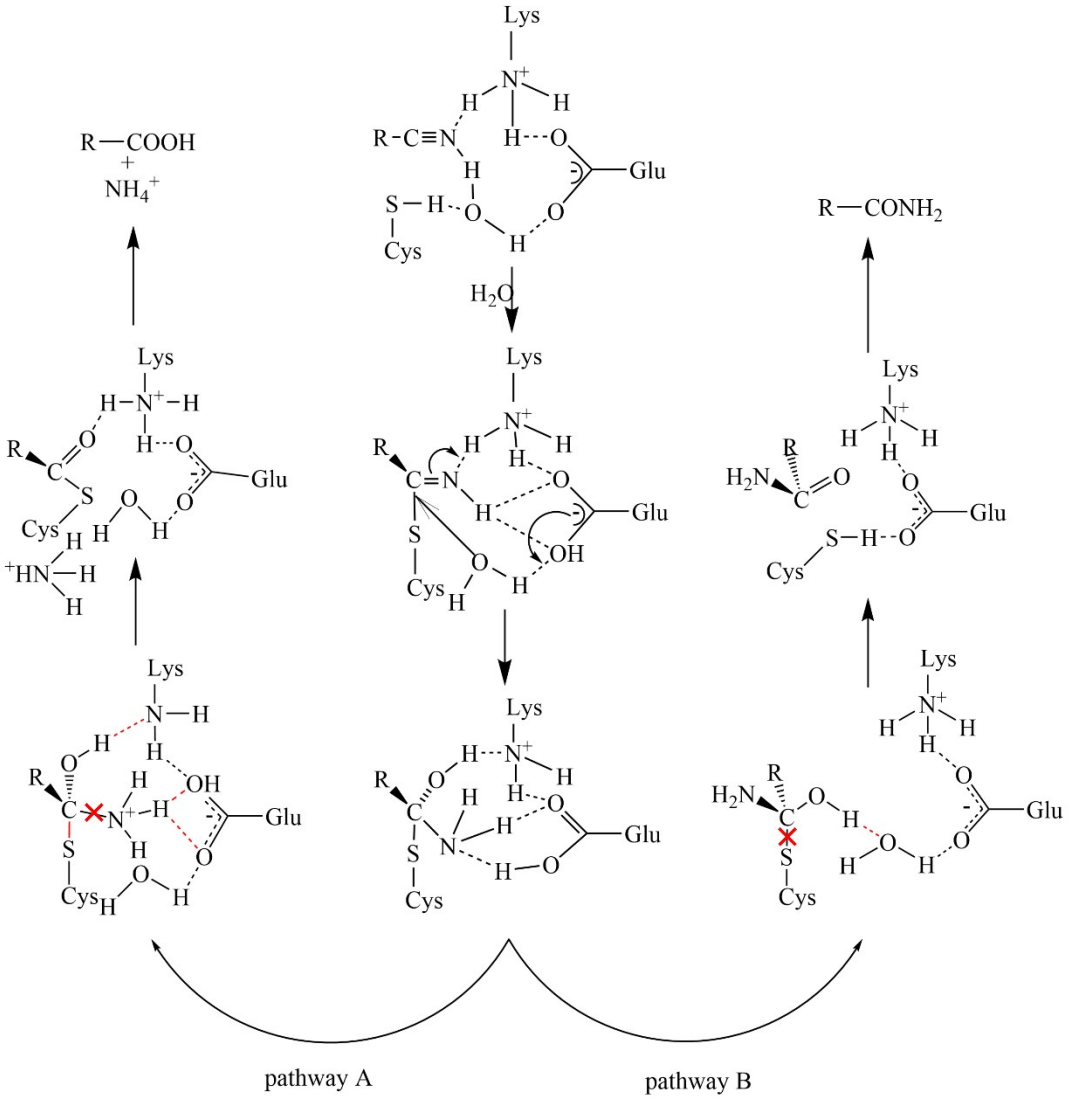

Figure S8. Catalytic mechanism of nitrilases. Nitrilases typically contain conserved catalytic residues Glu, Lys and Cys. Upon substrate entry into the active site, the thiol group of the Cys residue initially attacks the carbon atom of the substrate's cyano group, forming an enzyme-thioimidate complex. Subsequently, the Glu residue provides a proton that transfers to the enzyme-thioimidate complex; protonation of the nitrogen atom eliminates the imine structure, releasing NH_4^+ and generating one carboxylic acid molecule (pathway A). The proton donated by Glu combines with a solvent water molecule to form a nucleophile that attacks the intermediate. This transfers a proton to the Cys residue, hydrolyzing the thioester bond at the carbon of the cyano group to produce one amide molecule.

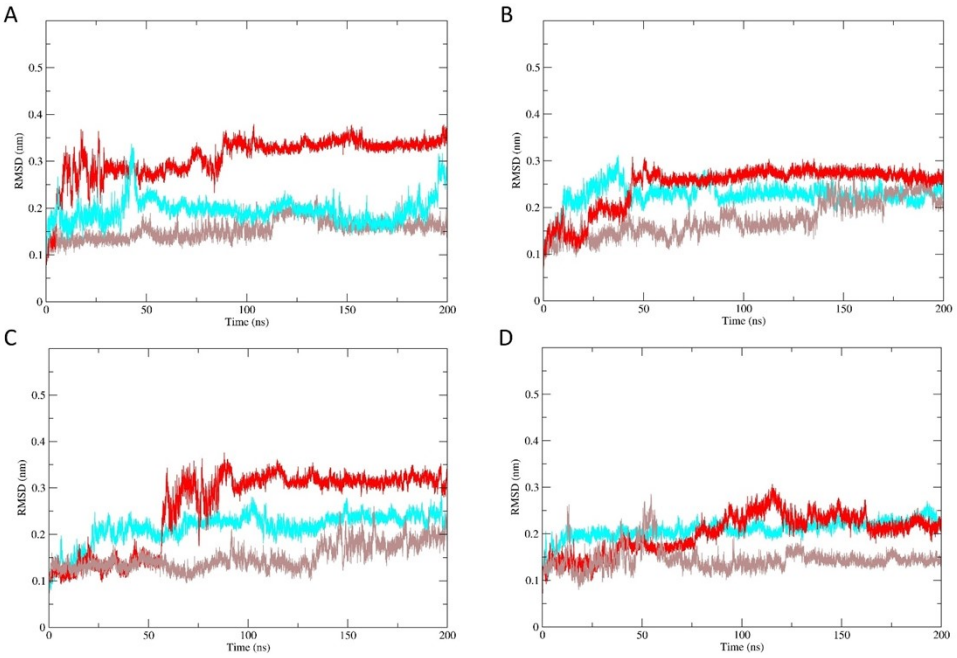

Figure S9. Root mean square deviation (RMSD) of WT-*R* (A), WT-*S* (B), T59D/F135L/R199W-*R* (C) and T59D/F135L/R199W-*S* (D). The RMSD was calculated from 200 ns MD simulation. All the MD simulations were repeated three independent times.

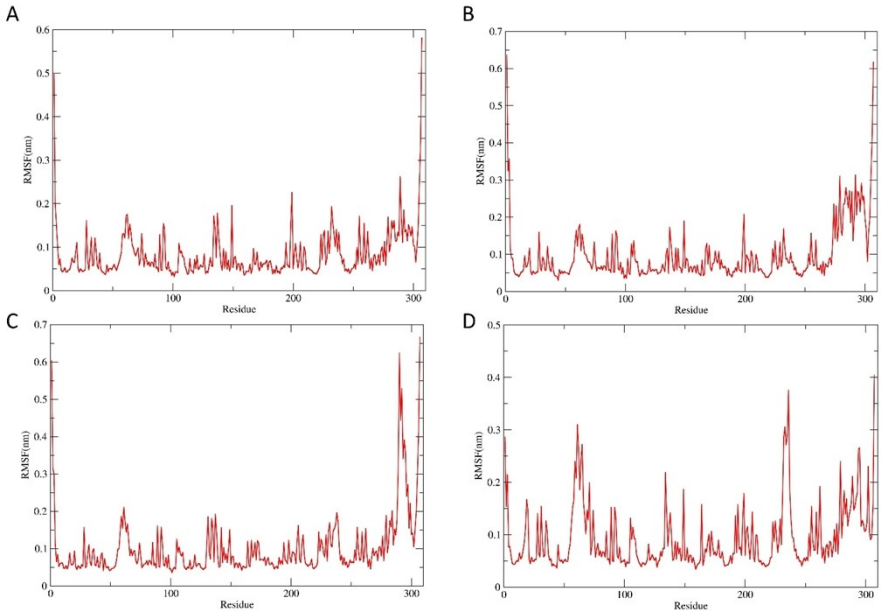

Figure S10. Root mean square fluctuation (RMSF) of WT-*R* (A), WT-*S* (B), T59D/F135L/R199W-*R* (C) and T59D/F135L/R199W-*S* (D). The residues were determined from last 50 ns of molecular dynamics (MD) simulations.

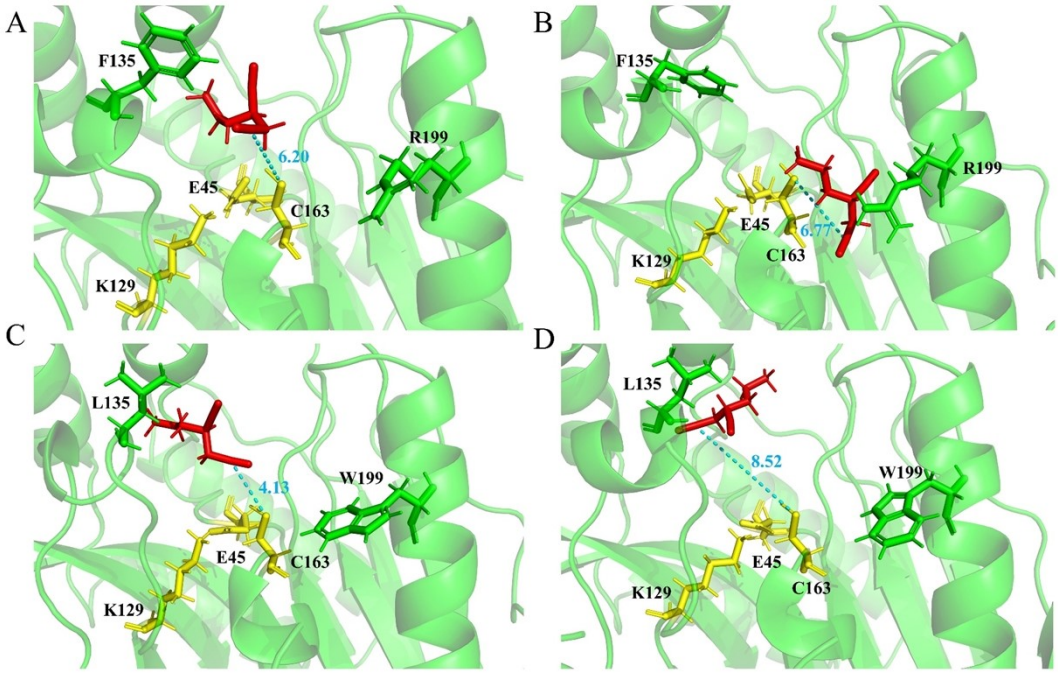

Figure S11. Characteristic distance (*D*c-s) representation of WT-*R* (A), WT-*S* (B), T59D/F135L/R199W-*R* (C), T59D/F135L/R199W-*S* (D). The catalytic triad residues E45, K129, and C163 are represented as yellow stick models, other residues as green stick models and cartoon representations, and substrate **1a** as red stick models.

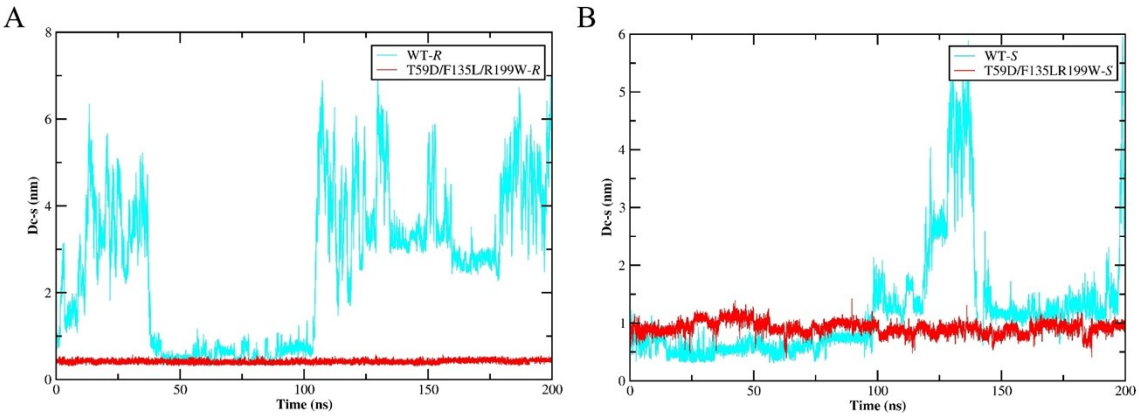

Figure S12. The distance between the thiol group of the catalytic triad cysteine and the carbon atoms on the cyano group of the substrate (*D*c-s) of the WT and T59D/F135L/R199W. (A) MD simulations of *D*c-s for WT-*R* and T59D/F135L/R199W-*R*. (B) MD simulations of *D*c-s for WT-*S* and T59D/F135L/R199W-*S*.

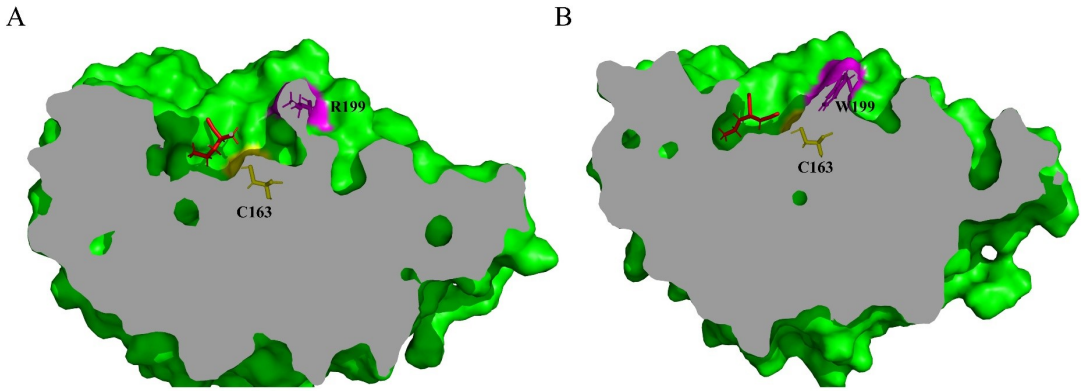

Figure S13. 3D structural sectional view of the enzyme. (A) The sectional view of WT-*R*. (B) The sectional view of T59D/F135L/R199W-*R*. The catalytic triad residue C163 is represented as yellow stick models, the mutant residue is represented as magenta stick models, and the substrate is represented as red stick models.

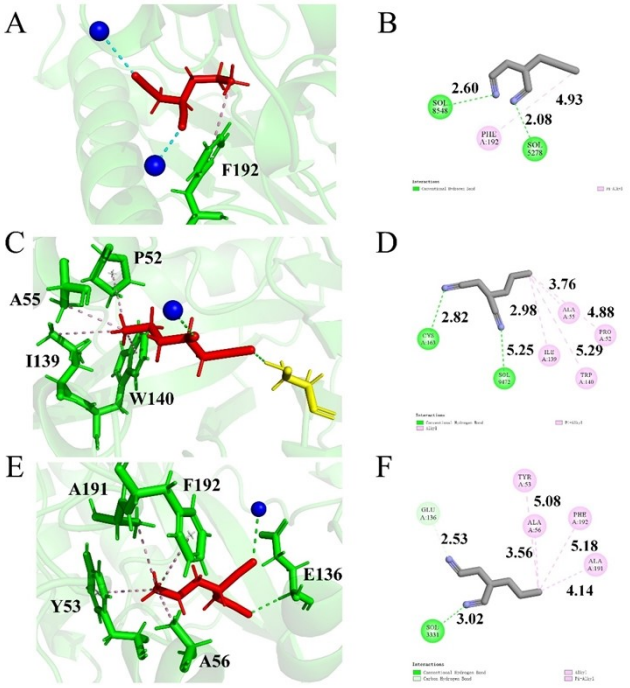

Figure S14. Interaction diagram of substrate with the active site of WT and T59D/F135L/R199W. (A) Interaction between (*R*)-**1a** (red) and WT (green). (B) 2D ligand interaction diagram of (*R*)-**1a** with WT. (C) Interaction between (*R*)-**1a** (red) and T59D/F135L/R199W (green cartoon). (D) 2D ligand interaction diagram of (*R*)-**1a** with T59D/F135L/R199W. (E) Interaction between (*S*)-**1a** (red) and T59D/F135L/R199W (green cartoon). (F) 2D ligand interaction diagram of (*S*)-**1a** with T59D/F135L/R199W. Water molecules are represented as blue spheres, hydrogen bonds are depicted as green dashed lines, and π-interactions are depicted as pink dashed lines.

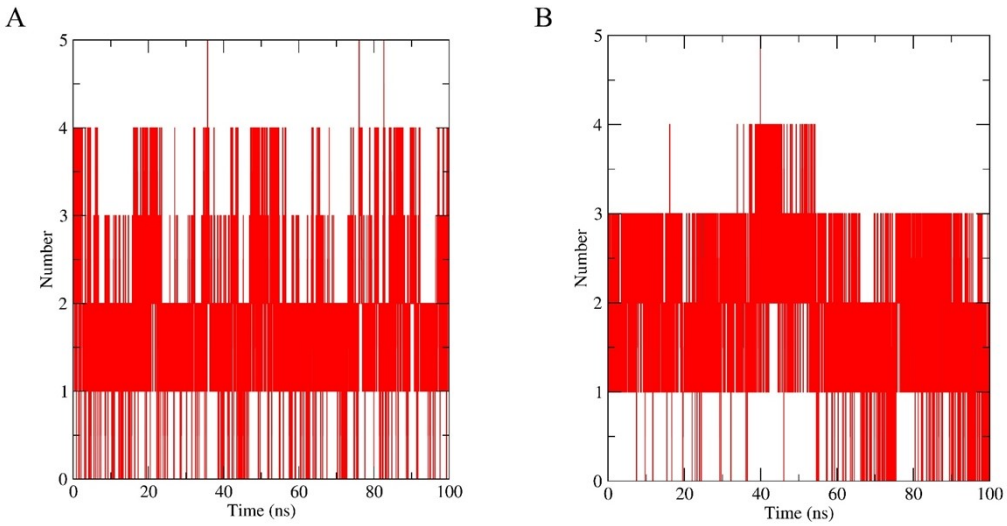

Figure S15. Number of hydrogen bonds for residue 59. (A) Number of hydrogen bonds formed between T59 and surrounding residues in the WT. (B) Number of hydrogen bonds formed between D59 and surrounding residues in T59D/F135L/R199W.

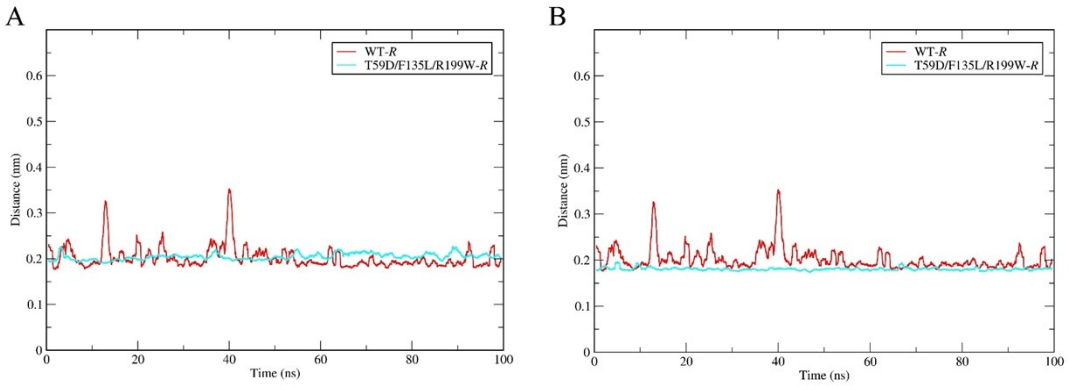

Figure S16. Hydrogen bond length between residues 61 and 65. (A) The fluctuation of the hydrogen bond length between the N-H of residue 65 and the O of residue 61. (B) The fluctuation of the hydrogen bond length between the O-H of residue 65 and the O of residue 61.

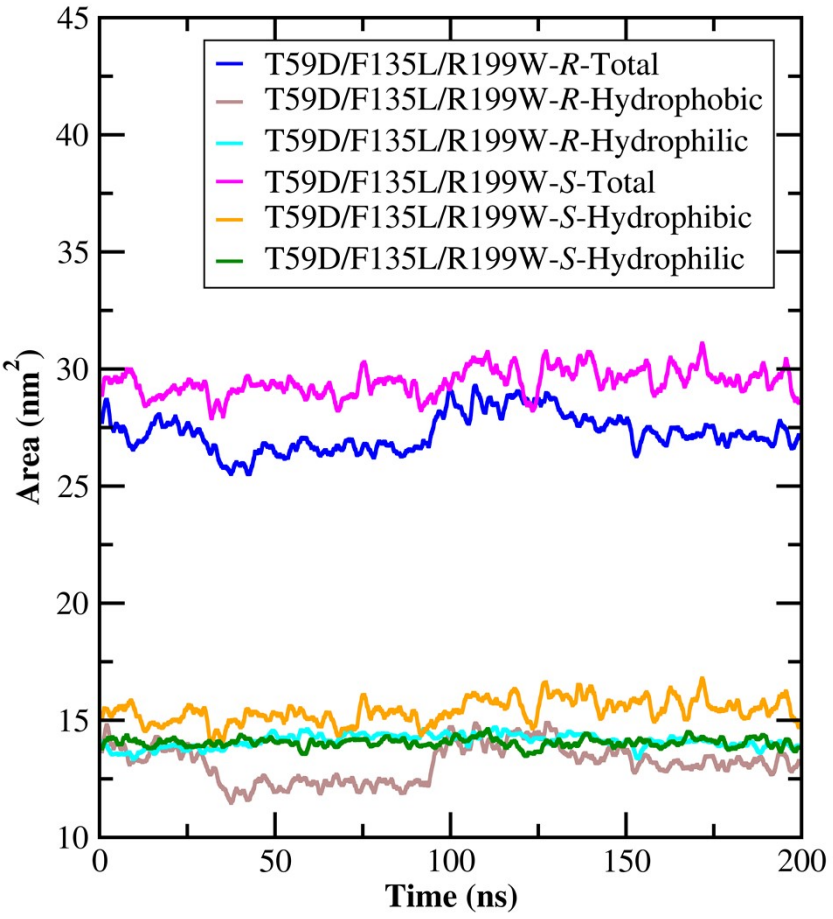

Figure S17. The fluctuation of the hydrophilic area and the hydrophobic area of T59D/F135L/R199W-*R* and T59D/F135L/R199W-*S*.

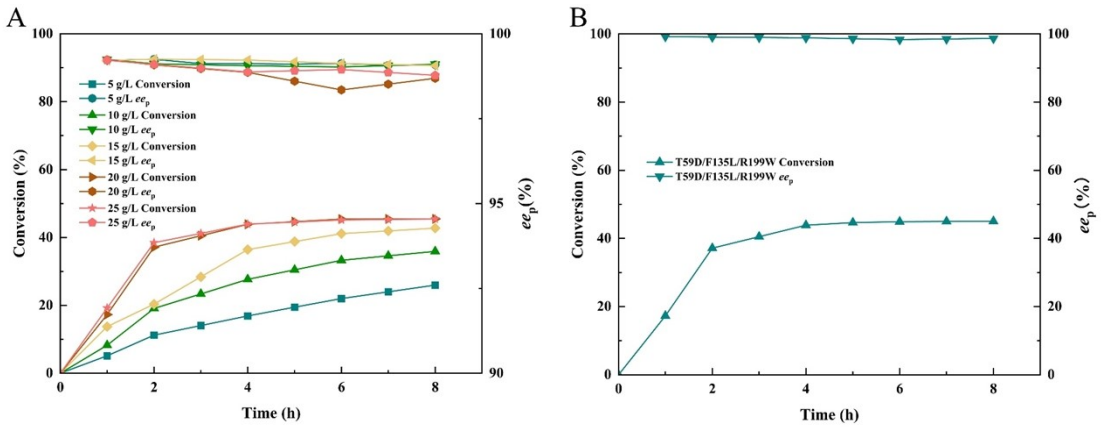

Figure S18. The reaction process of desymmetrizing hydrolysis of **1a** by T59D/F135L/R199W. (A) The reaction process of different concentrations of recombinant cells as biocatalyst. (B) The reaction process of 20 g/L recombinant cells as biocatalyst at 3 L scale.

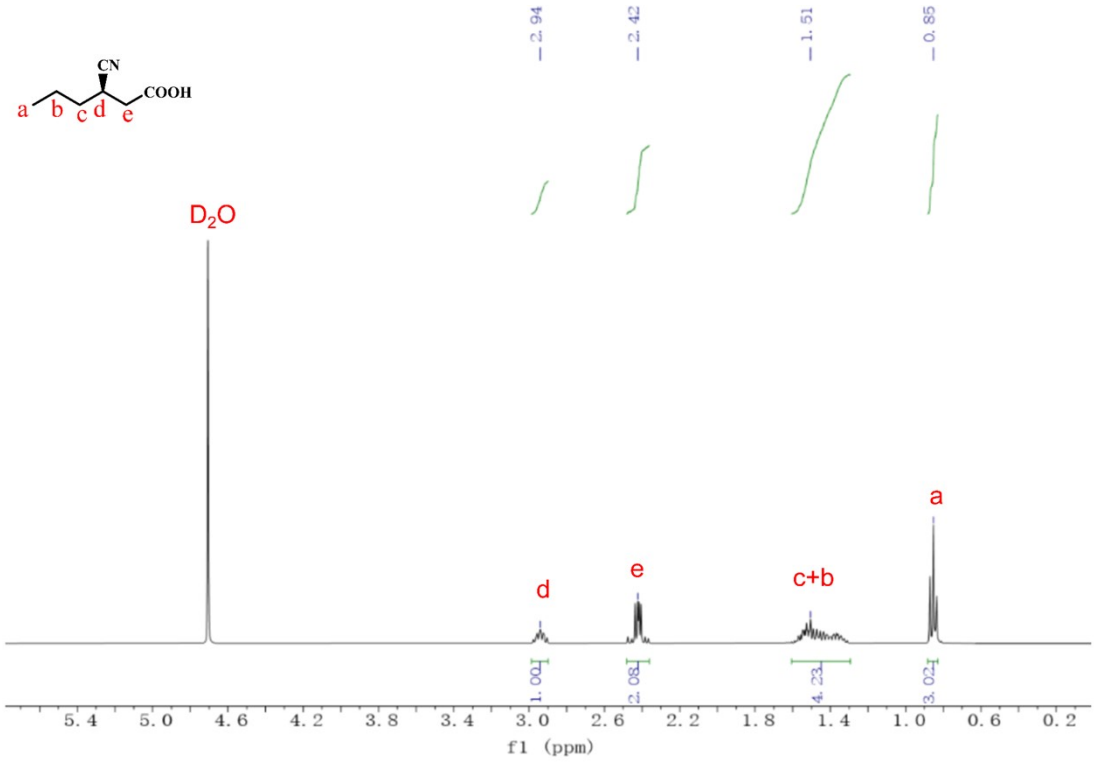

Figure S19. ^{1}H NMR of (*R*)-**2a**. ^{1}H NMR (400 MHz, D_2O) δ: 3.00–2.88 (m, 1H), 2.50–2.34 (m, 2H), 1.63–1.27 (m, 4H), 0.85 (t, 3H).

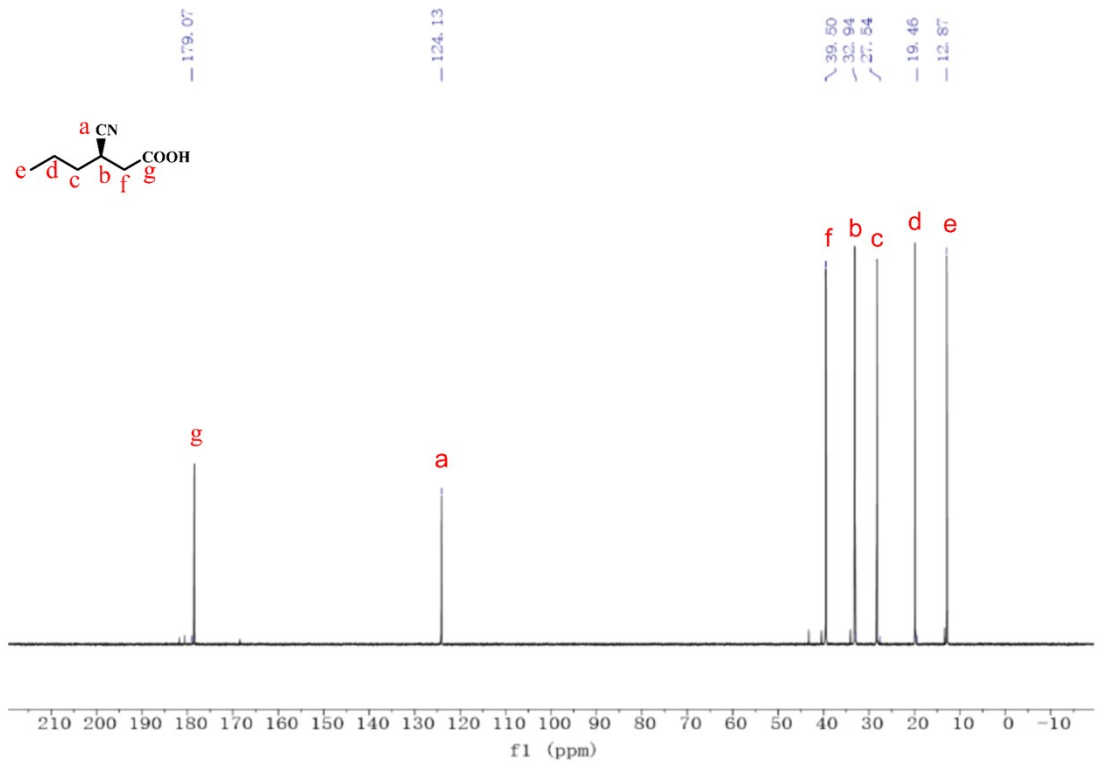

Figure S20. ^{13}C NMR of (*R*)-**2a**. ^{13}C NMR (400 MHz, D_2O) δ: 179.07, 124.13, 39.50, 32.94, 27.54, 19.46, 12.87.

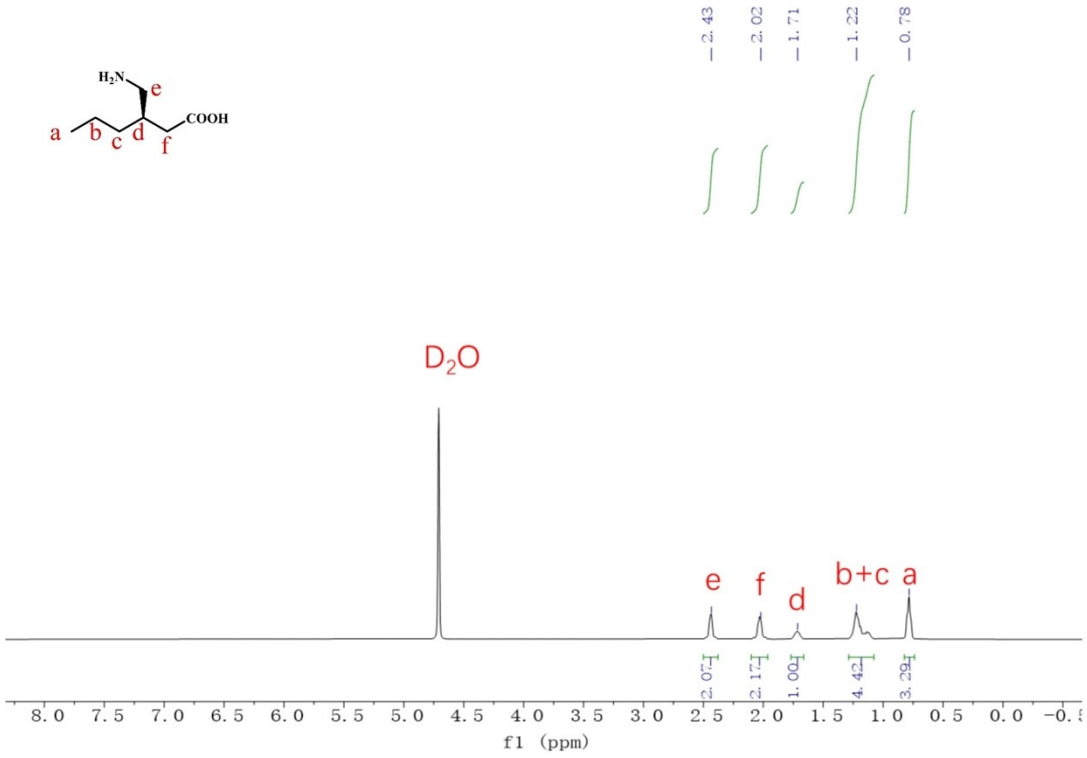

Figure S21. ^{1}H NMR of **5**. ^{1}H NMR (400 MHz, D_2O) δ: 2.51–2.37 (m, 2H), 2.02 (d, 2H), 1.71 (m, 1H), 1.22 (m, 2H), 1.13 (m, 2H), 0.78 (t, 3H).

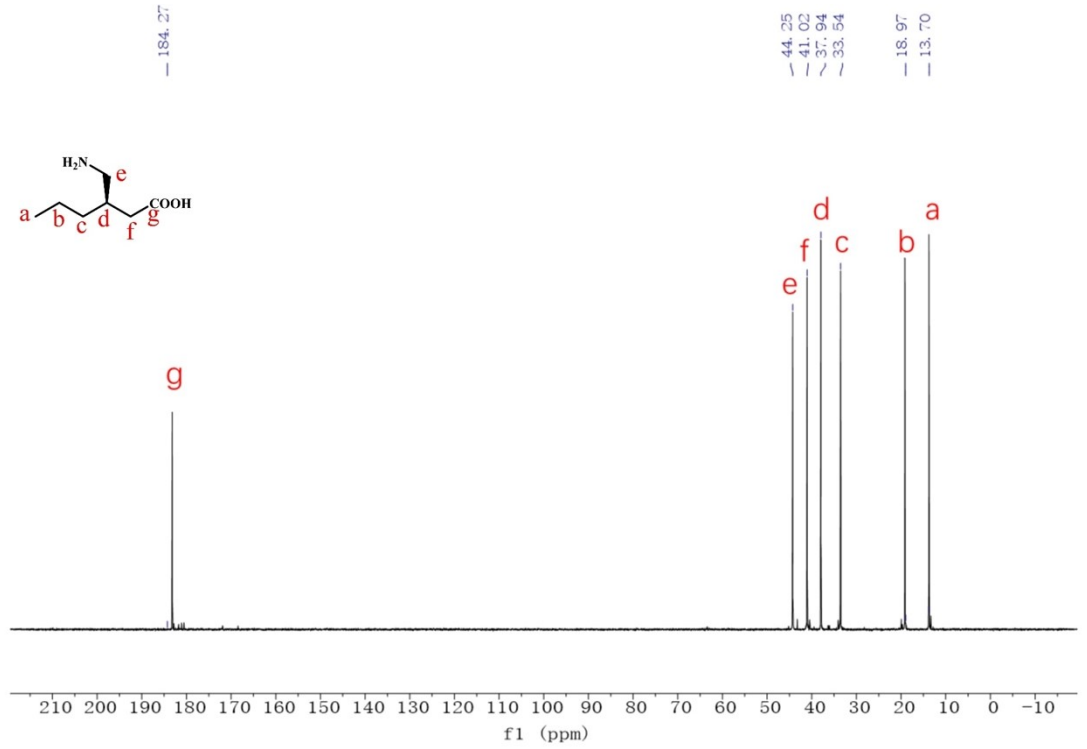

Figure S22. ^{13}C NMR of **5**. ^{13}C NMR (400 MHz, D_2O) δ: 184.27, 44.25, 41.02, 37.94, 33.54, 18.97, 13.70.

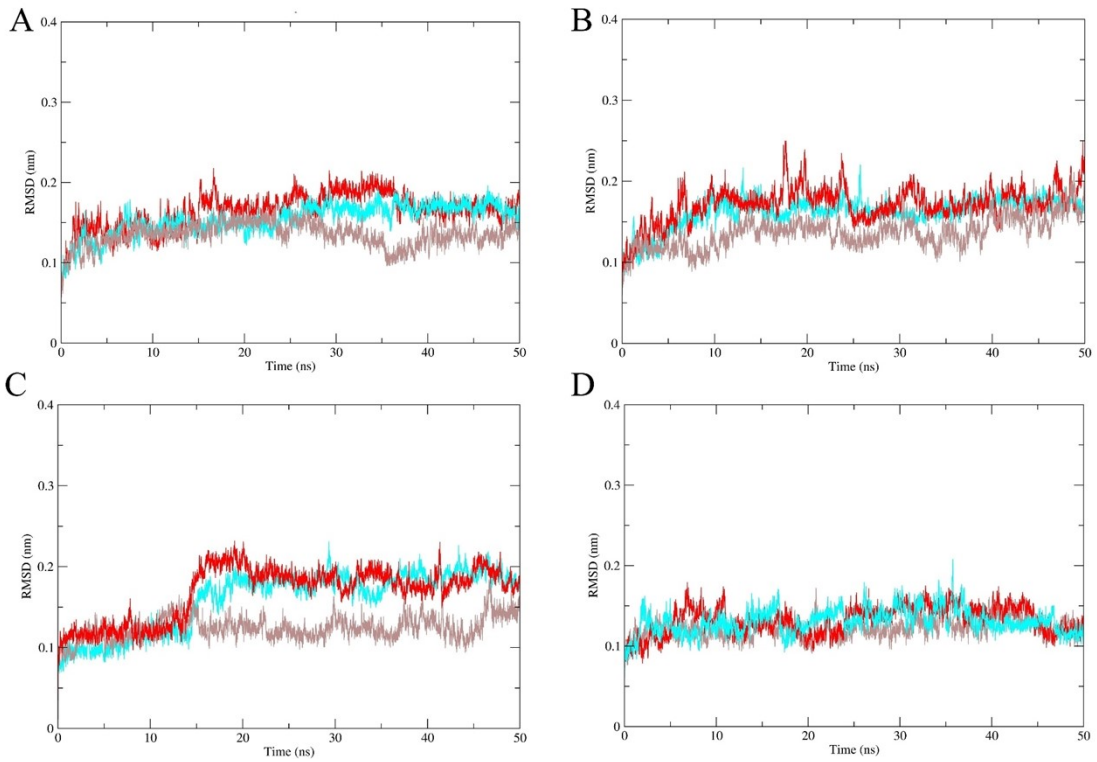

Figure S23. RMSD of (*R*)-**1b** binding in WT (A), (*S*)-1b binding in WT (B), (*R*)-**1b** binding in T59D/F135L/R199W (C) and (*S*)-**1b** binding in T59D/F135L/R199W (D). The RMSD was calculated from a 50 ns MD simulation. All the MD simulations were repeated three independent times.

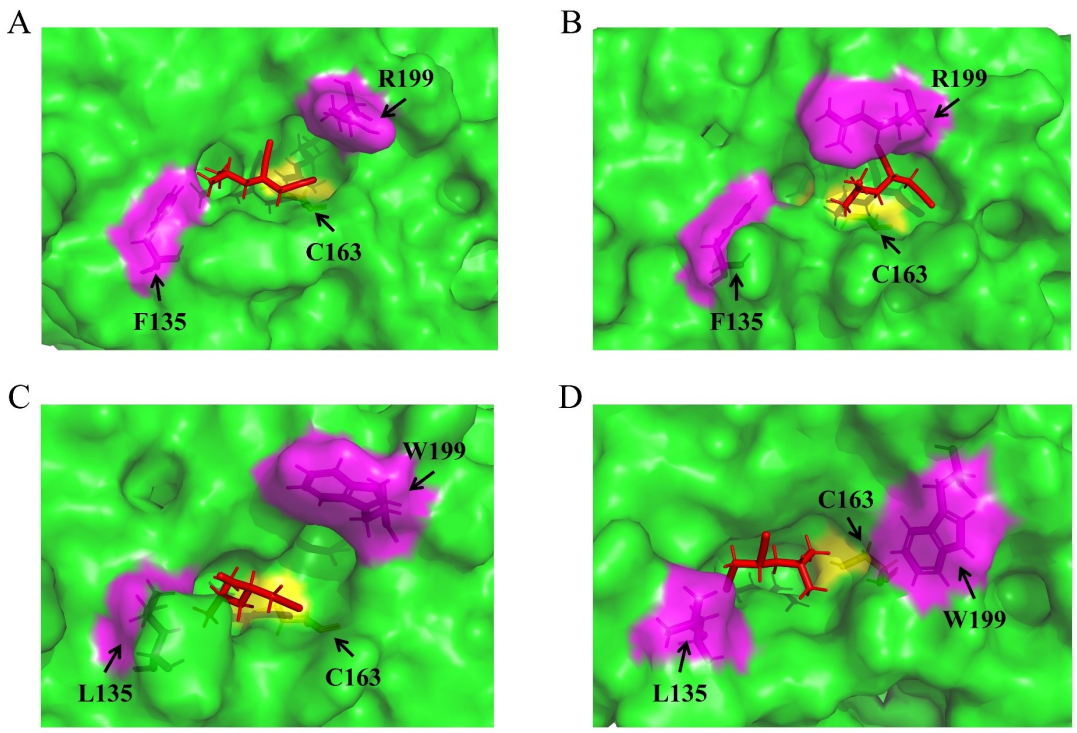

Figure S24. Surface diagram of characteristic structure representation of (*R*)-**1b** binding in WT (A), (*S*)-**1b** binding in WT (B), (*R*)-**1b** binding in T59D/F135L/R199W (C) and (*S*)-**1b** binding in T59D/F135L/R199W (D). Mutant residues are shown as magenta sticks and surface. The substrate **1a** is shown as red sticks. The catalytic triad residue C163 is shown as a yellow stick and surface.

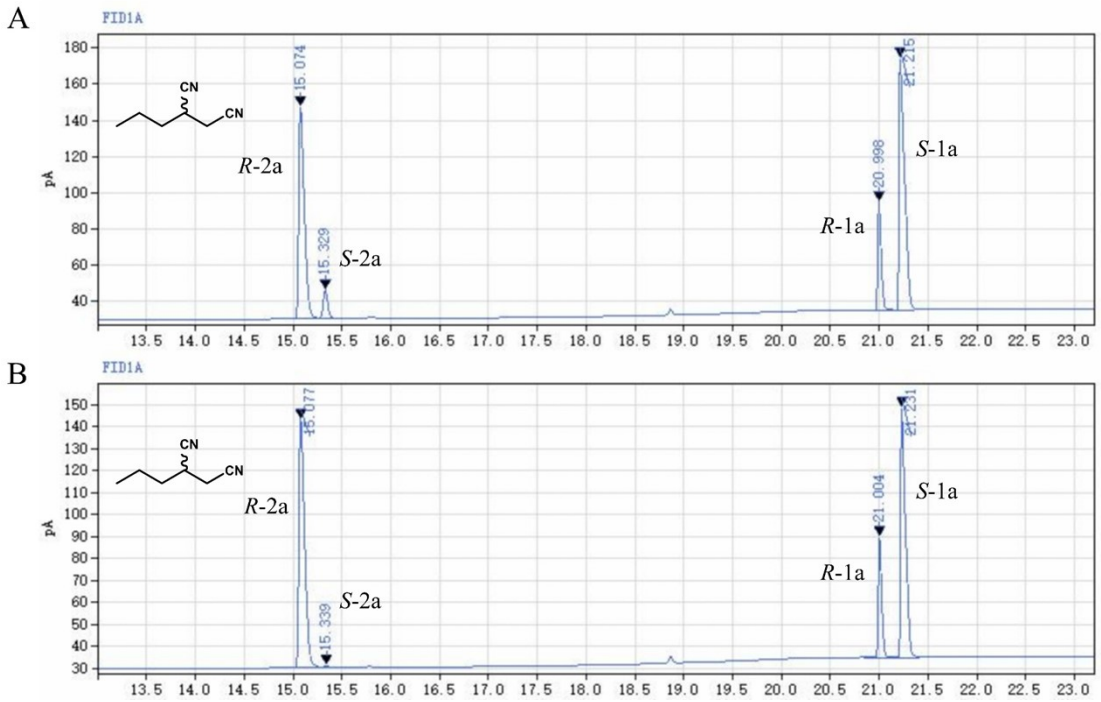

Figure S25. GC analysis of the kinetic resolution of **1a** by WT (A) and T59D/F135L/R199W (B). GC-FID analysis was performed on a BGB-175 column (30 m × 0.25 mm, 0.25 μm) with nitrogen as carrier gas. The GC-FID conditions were as follows: injector and detector temperatures at 250 °C; oven temperature held at 120 °C for 12 min, ramped at 10 °C·min^{-1} to 200 °C, and held for 5 min.

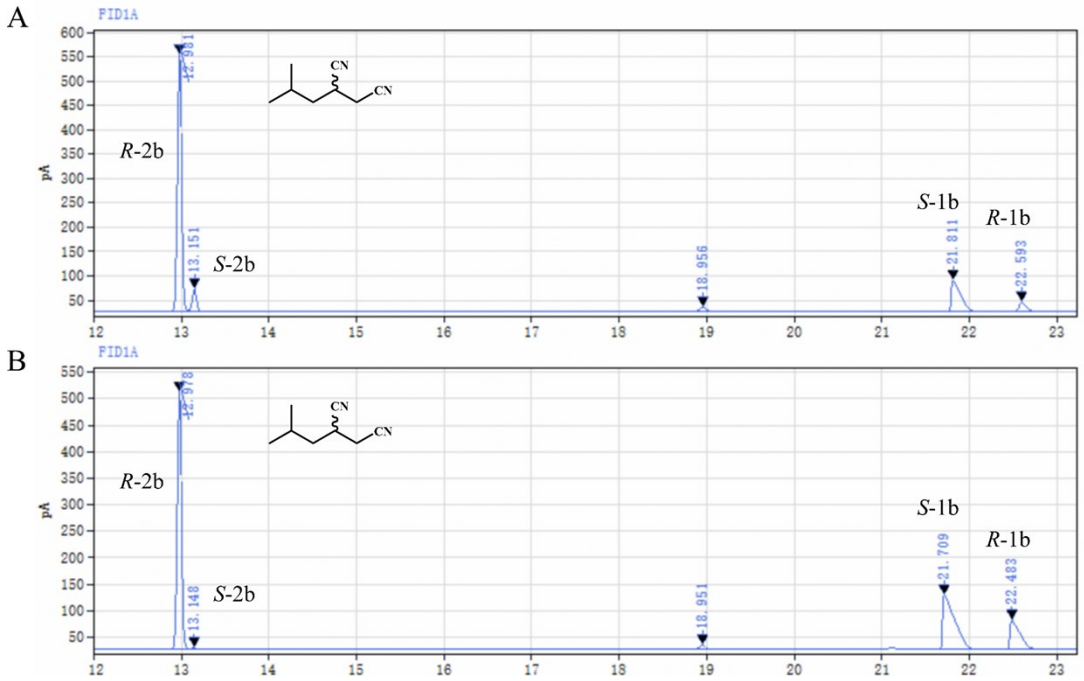

Figure S26. GC analysis of the kinetic resolution of **1b** by WT (A) and T59D/F135L/R199W (B). GC-FID analysis was performed on a BGB-174 column (30 m × 0.25 mm, 0.25 μm) with nitrogen as carrier gas. The GC-FID conditions were as follows: injector and detector temperatures at 250 °C; oven temperature held at 120 °C for 15 min, ramped at 10 °C·min^{-1} to 170 °C, and held for 10 min, ramped at 10 °C·min^{-1} to 200 °C, and held for 7 min.

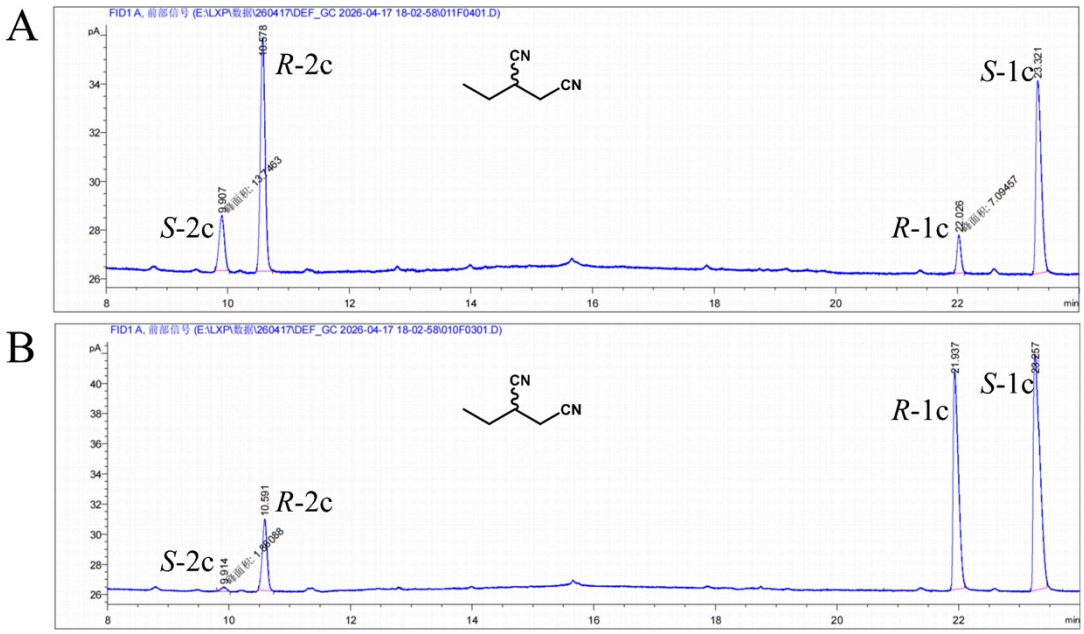

Figure S27. GC analysis of the kinetic resolution of 1c by WT (A) and T59D/F135L/R199W (B). GC-FID analysis was performed on a BGB-174 column (30 m × 0.25 mm, 0.25 μm) with nitrogen as carrier gas. The GC-FID conditions were as follows: injector and detector temperatures at 250 °C; oven temperature held at 120 °C for 15 min, ramped at 10 °C·min^{-1} to 170 °C, and held for 10 min, ramped at 10 °C·min^{-1} to 200 °C, and held for 7 min.

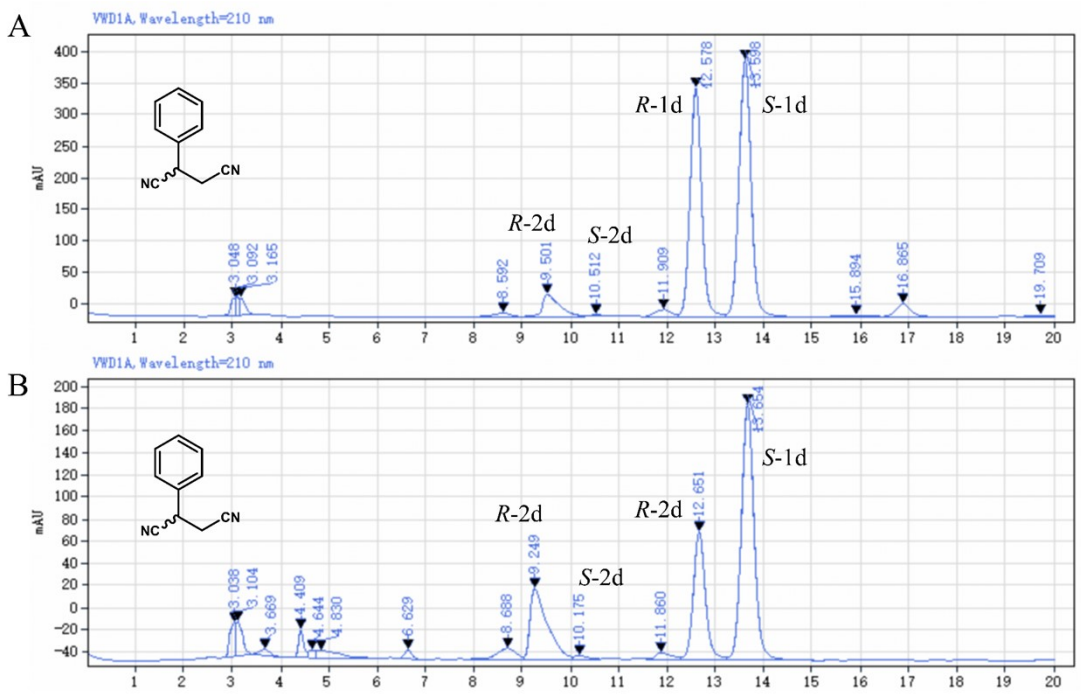

Figure S28. HPLC analysis of the kinetic resolution of **1d** by WT (A) and T59D/F135L/R199W (B). Chiral HPLC: DAICEL AD-H, 210 nm, n-hexane/isopropanol = 90:10, flow rate 1 mL/min.

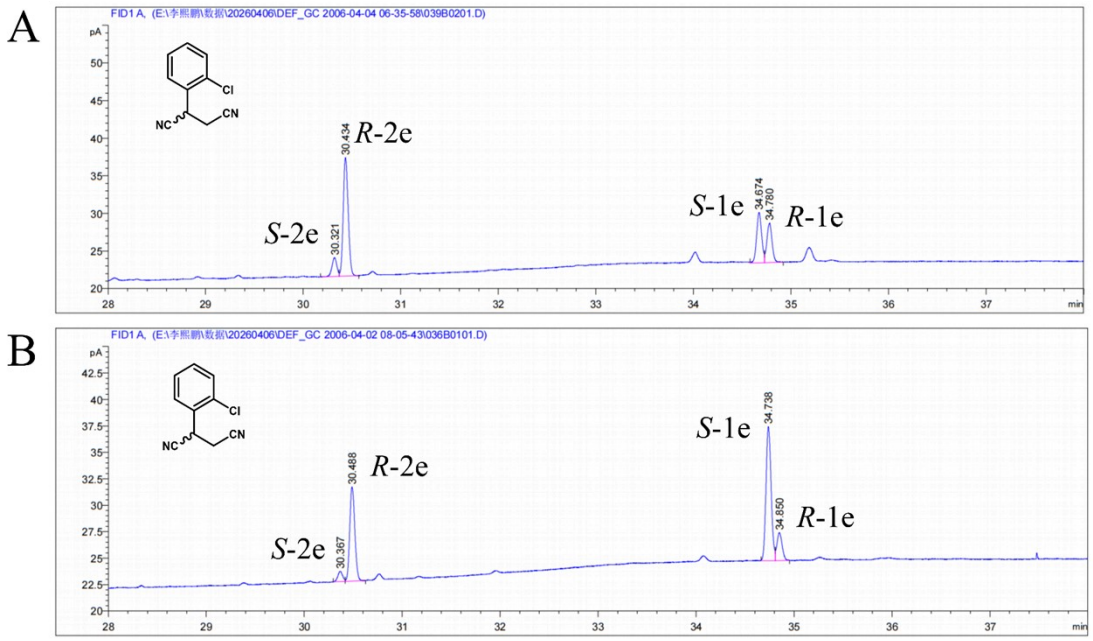

Figure S29. GC analysis of the kinetic resolution of **1e** by WT (A) and T59D/F135L/R199W (B). GC-FID analysis was performed on a BGB-175 column (30 m × 0.25 mm, 0.25 μm) with nitrogen as carrier gas. The GC-FID conditions were as follows: injector and detector temperatures at 250 °C; oven temperature held at 80 °C for 5 min, ramped at 5 °C·min^{-1} to 220 °C, and held for 10 min.

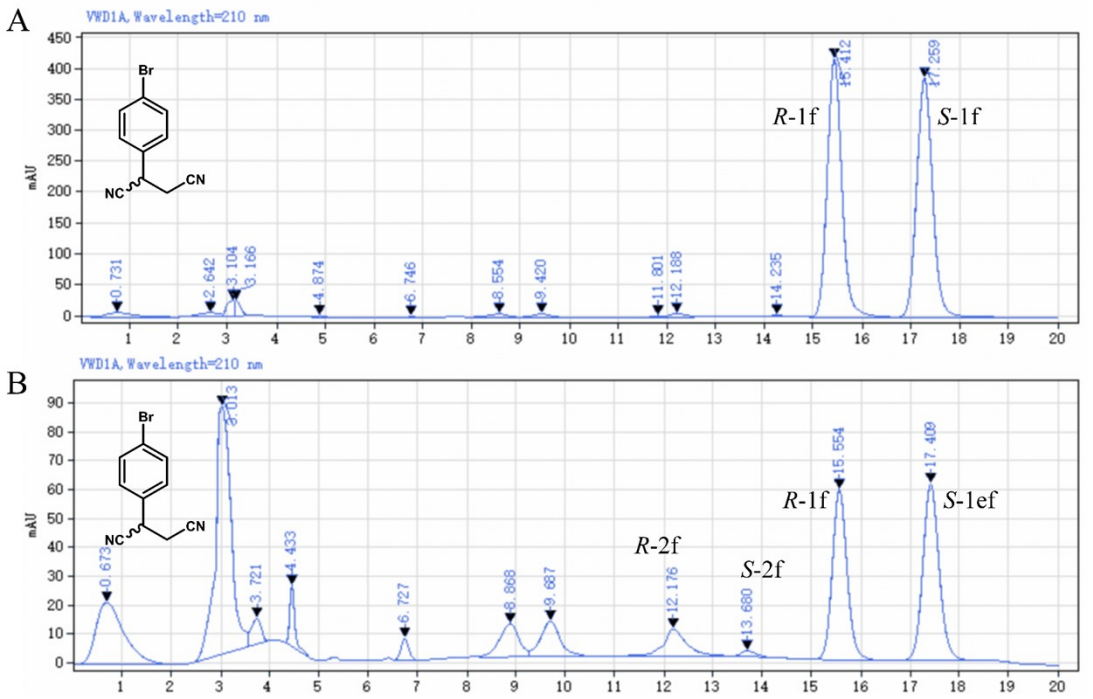

Figure S30. HPLC analysis of the kinetic resolution of **1f** by WT (A) and T59D/F135L/R199W (B). Chiral HPLC: DAICEL AD-H, 210 nm, n-hexane/isopropanol = 90:10, flow rate 1 mL/min.

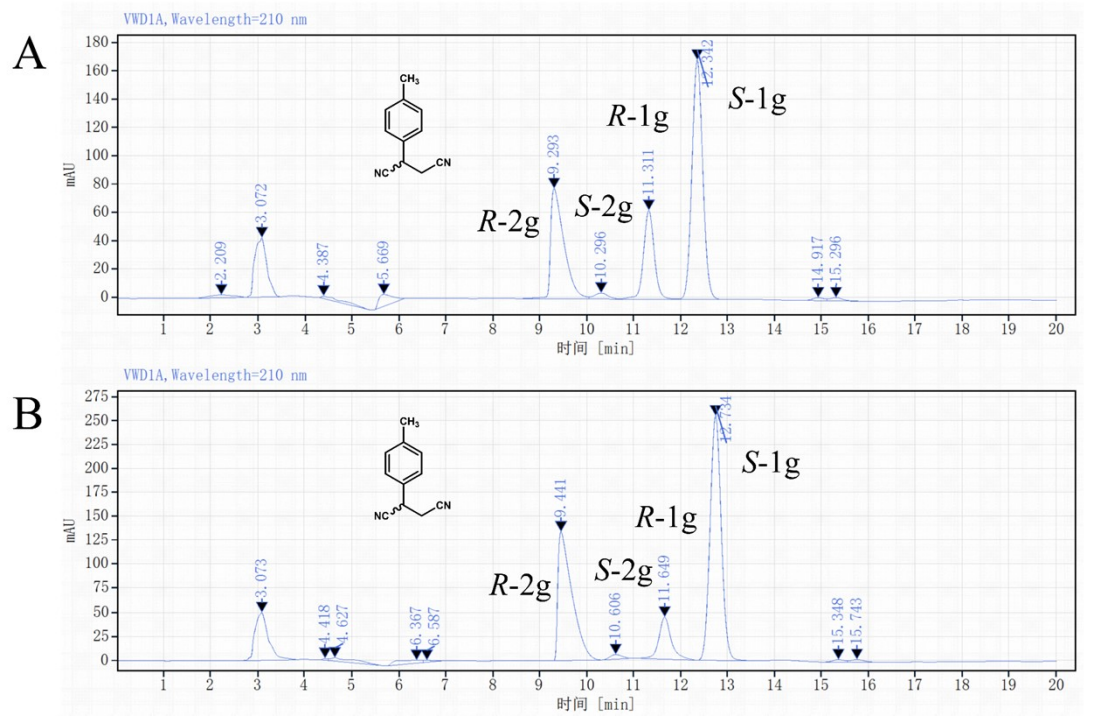

Figure S31. HPLC analysis of the kinetic resolution of **1g** by WT (A) and T59D/F135L/R199W (B). Chiral HPLC: DAICEL AD-H, 210 nm, n-hexane/isopropanol = 90:10, flow rate 1 mL/min.

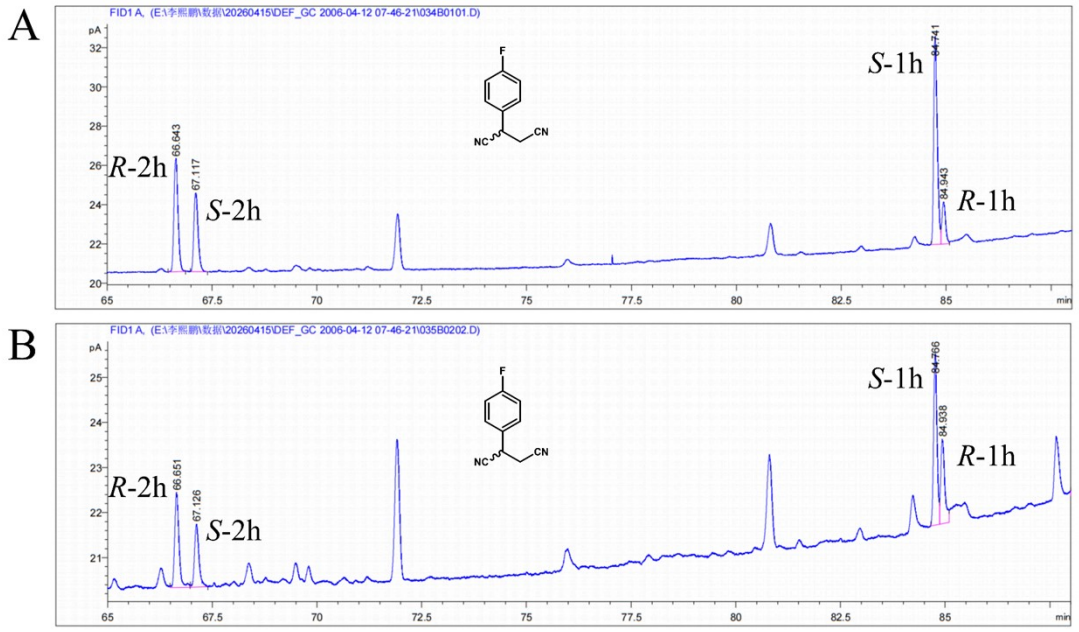

Figure S32. GC analysis of the kinetic resolution of **1h** by WT (A) and T59D/F135L/R199W (B). GC-FID analysis was performed on a BGB-175 column (30 m × 0.25 mm, 0.25 μm) with nitrogen as carrier gas. The GC-FID conditions were as follows: injector and detector temperatures at 250 °C; oven temperature held at 60 °C for 10 min, ramped at 2 °C·min^{-1} to 220 °C, and held for 10 min.

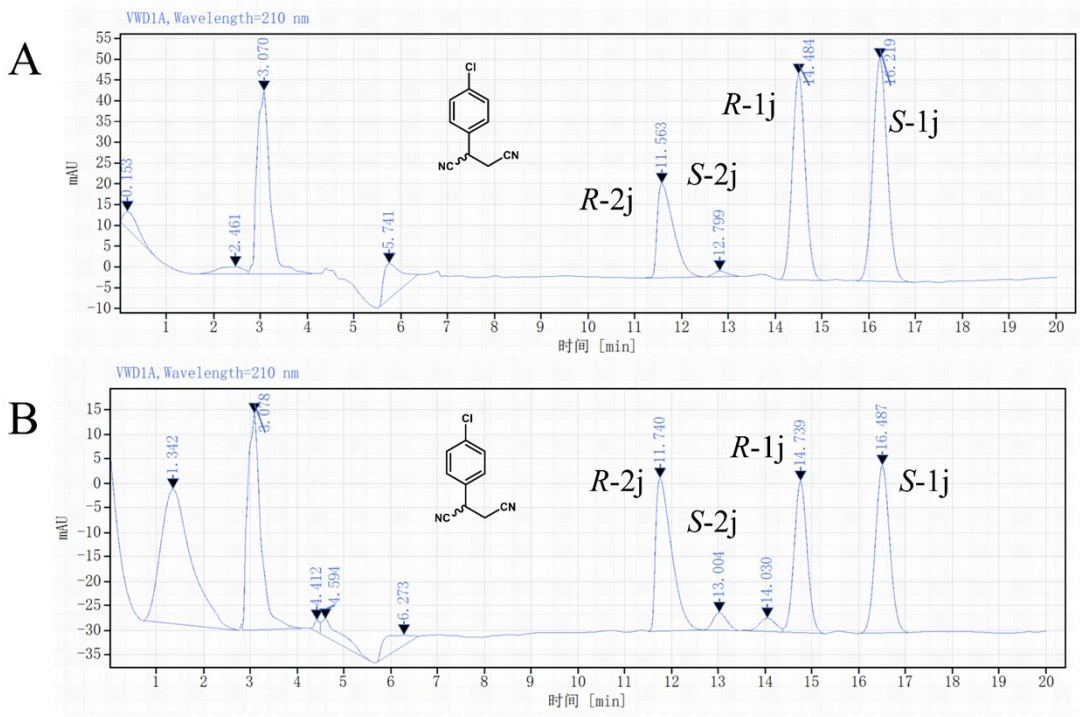

Figure S33. HPLC analysis of the kinetic resolution of **1j** by WT (A) and T59D/F135L/R199W (B). Chiral HPLC: DAICEL AD-H, 210 nm, n-hexane/isopropanol = 90:10, flow rate 1 mL/min.

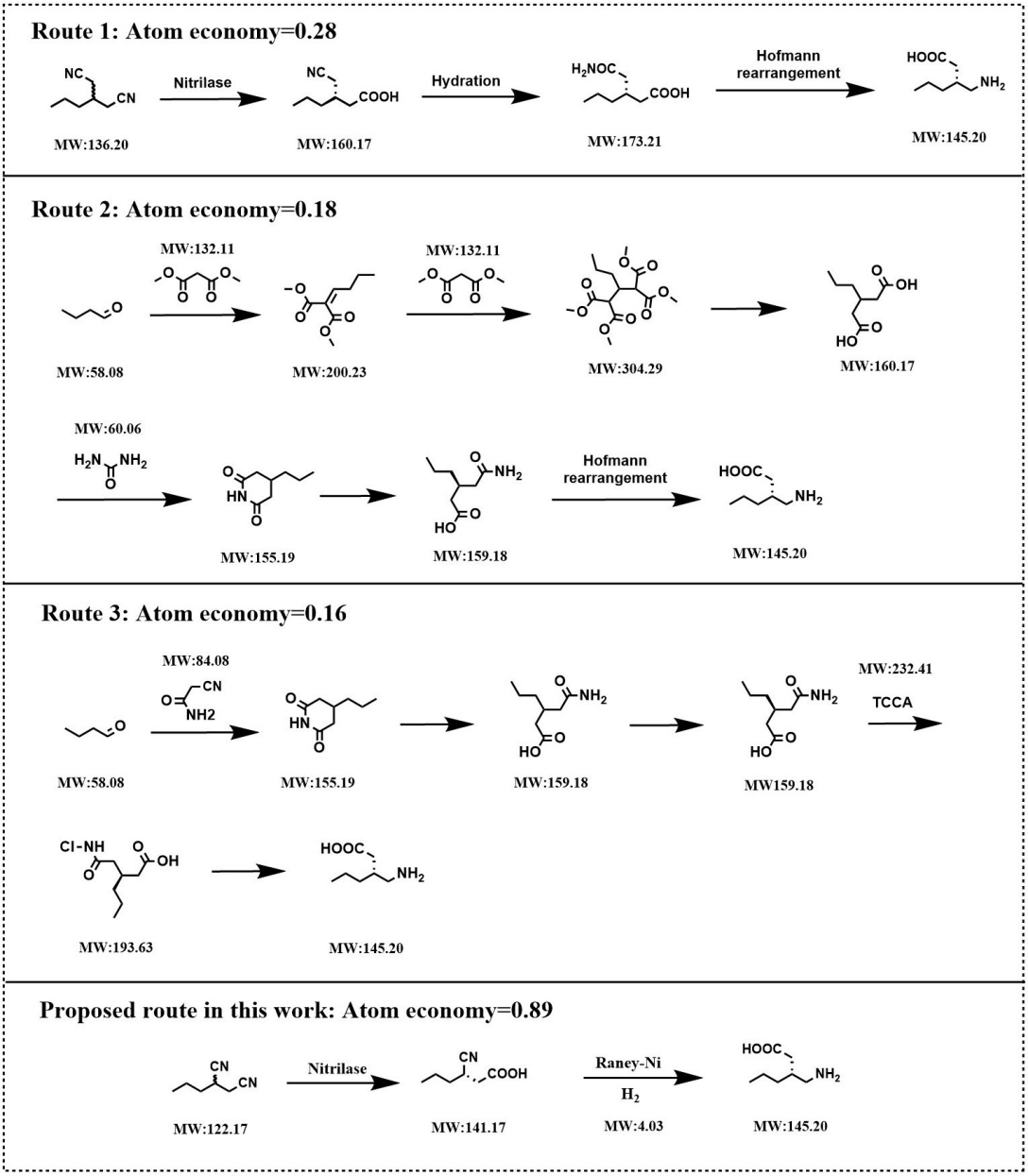

Figure S34. Comparison of different synthetic routes for the key intermediate of Brivaracetam. TCCA = trichloroisocyanuric acid.

The DNA sequence of *Pg*NIT and other main variants.

*Pg*NIT:

ATGGGTAAAGTTGTCAAAGCCGCTGCTGTTCAATTTTCTCCAGTTCTGTACAGCCGCGAA
GCAACCGTAGCAAAAGTCGTACAGAAGATCCACGAACTGGGTCTGAAAGGCGTGCAATT
CGCTACCTTCCCGGAAACCGTTGTCCCGTACTACCCGTATTTCGCTGCAGTTCAGACTG
GTATCGAGCTGCTGAGCGGTTCCGAACACCTGCGTCTGCTGGAGCAGGCGGTTACTGT
TCCTAGCGCGGCTACGGATGCAATCGGTAAAGCTGCTCGTGAAGCAGGTATGGTTGTAT
CTATCGGCGTGAACGAGCGCGACGGTGGCACGCTGTACAACACCCAACTGCTGTTTGAT
GCCGATGGCACGCTGATTCAGCGTCGCCGTAAAATCACCCCAACTCACTTCGAACGTAT
GATTTGGGGTCAGGGTGATGGTTCTGGTCTGCGTGCGGTTGATTCCGCCGTGGGCCGC
ATTGGTCAGCTGGCGTGTTTCGAACATAACAACCCACTGGCCCGTTACGCGATGATCGC

TGATGGCGAACAAATCCATTCTGCGATGTATCCGGGCAGCGCTTTTGGCGAAGGTTTTG
CGCAGCGTATGGAAATCAACATTCGTCAGCACGCACTGGAATCCGGCGCGTTCGTAGTC
AACGCAACCGCATGGCTGGATGCGGATCAGCAGGCACAAATTATGAAAGACACCGGCT
GCGGCATTGGTCCAATTAGCGGTGGTTGTTTCACCACCATTGTTTCCCCGGACGGTATG
CTGATGGCTGAACCGCTGCGCTCTGGTGAGGGCGAGGTCATCGTTGACCTGGACTTTG
CACAGATCGATCGTCGTAAAATGCTGATGGACGCTGCCGGTCATTACAACCGTCCGGAA
CTGCTGTCTCTGATGATCGATCGTACCCCTACCGCGCATGTACATGAACGTGCGCCGCA
CTCCCTGCCGGTAAGCGACAAAGCGGACGACGACGTGCGCACCCAAGCGGCTGCAGTC
GCGGGTTCCCGCCTCGAGATT

F135L:
ATGGGTAAAGTTGTCAAAGCCGCTGCTGTTCAATTTTCTCCAGTTCTGTACAGCCGCGAA
GCAACCGTAGCAAAAGTCGTACAGAAGATCCACGAACTGGGTCTGAAAGGCGTGCAATT
CGCTACCTTCCCGGAAACCGTTGTCCCGTACTACCCGTATTTCGCTGCAGTTCAGACTG
GTATCGAGCTGCTGAGCGGTTCCGAACACCTGCGTCTGCTGGAGCAGGCGGTTACTGT
TCCTAGCGCGGCTACGGATGCAATCGGTAAAGCTGCTCGTGAAGCAGGTATGGTTGTAT
CTATCGGCGTGAACGAGCGCGACGGTGGCACGCTGTACAACACCCAACTGCTGTTTGAT
GCCGATGGCACGCTGATTCAGCGTCGCCGTAAAATCACCCCAACTCACCTGGAACGTAT
GATTTGGGGTCAGGGTGATGGTTCTGGTCTGCGTGCGGTTGATTCCGCCGTGGGCCGC
ATTGGTCAGCTGGCGTGTTTCGAACATAACAACCCACTGGCCCGTTACGCGATGATCGC
TGATGGCGAACAAATCCATTCTGCGATGTATCCGGGCAGCGCTTTTGGCGAAGGTTTTG
CGCAGCGTATGGAAATCAACATTCGTCAGCACGCACTGGAATCCGGCGCGTTCGTAGTC
AACGCAACCGCATGGCTGGATGCGGATCAGCAGGCACAAATTATGAAAGACACCGGCT
GCGGCATTGGTCCAATTAGCGGTGGTTGTTTCACCACCATTGTTTCCCCGGACGGTATG
CTGATGGCTGAACCGCTGCGCTCTGGTGAGGGCGAGGTCATCGTTGACCTGGACTTTG
CACAGATCGATCGTCGTAAAATGCTGATGGACGCTGCCGGTCATTACAACCGTCCGGAA
CTGCTGTCTCTGATGATCGATCGTACCCCTACCGCGCATGTACATGAACGTGCGCCGCA
CTCCCTGCCGGTAAGCGACAAAGCGGACGACGACGTGCGCACCCAAGCGGCTGCAGTC
GCGGGTTCCCGCCTCGAGATT

F135L/R199W:
ATGGGTAAAGTTGTCAAAGCCGCTGCTGTTCAATTTTCTCCAGTTCTGTACAGCCGCGAA
GCAACCGTAGCAAAAGTCGTACAGAAGATCCACGAACTGGGTCTGAAAGGCGTGCAATT
CGCTACCTTCCCGGAAACCGTTGTCCCGTACTACCCGTATTTCGCTGCAGTTCAGACTG
GTATCGAGCTGCTGAGCGGTTCCGAACACCTGCGTCTGCTGGAGCAGGCGGTTACTGT
TCCTAGCGCGGCTACGGATGCAATCGGTAAAGCTGCTCGTGAAGCAGGTATGGTTGTAT
CTATCGGCGTGAACGAGCGCGACGGTGGCACGCTGTACAACACCCAACTGCTGTTTGAT
GCCGATGGCACGCTGATTCAGCGTCGCCGTAAAATCACCCCAACTCACCTGGAACGTAT
GATTTGGGGTCAGGGTGATGGTTCTGGTCTGCGTGCGGTTGATTCCGCCGTGGGCCGC
ATTGGTCAGCTGGCGTGTTTCGAACATAACAACCCACTGGCCCGTTACGCGATGATCGC
TGATGGCGAACAAATCCATTCTGCGATGTATCCGGGCAGCGCTTTTGGCGAAGGTTTTG
CGCAGTGGATGGAAATCAACATTCGTCAGCACGCACTGGAATCCGGCGCGTTCGTAGTC
AACGCAACCGCATGGCTGGATGCGGATCAGCAGGCACAAATTATGAAAGACACCGGCT

GCGGCATTGGTCCAATTAGCGGTGGTTGTTTCACCACCATTGTTTCCCCGGACGGTATG
CTGATGGCTGAACCGCTGCGCTCTGGTGAGGGCGAGGTCATCGTTGACCTGGACTTTG
CACAGATCGATCGTCGTAAAATGCTGATGGACGCTGCCGGTCATTACAACCGTCCGGAA
CTGCTGTCTCTGATGATCGATCGTACCCCTACCGCGCATGTACATGAACGTGCGCCGCA
CTCCCTGCCGGTAAGCGACAAAGCGGACGACGACGTGCGCACCCAAGCGGCTGCAGTC
GCGGGTTCCCGCCTCGAGATT

F135L/R199W/T59D:
ATGGGTAAAGTTGTCAAAGCCGCTGCTGTTCAATTTTCTCCAGTTCTGTACAGCCGCGAA
GCAACCGTAGCAAAAGTCGTACAGAAGATCCACGAACTGGGTCTGAAAGGCGTGCAATT
CGCTACCTTCCCGGAAACCGTTGTCCCGTACTACCCGTATTTCGCTGCAGTTCAGGACG
GTATCGAGCTGCTGAGCGGTTCCGAACACCTGCGTCTGCTGGAGCAGGCGGTTACTGT
TCCTAGCGCGGCTACGGATGCAATCGGTAAAGCTGCTCGTGAAGCAGGTATGGTTGTAT
CTATCGGCGTGAACGAGCGCGACGGTGGCACGCTGTACAACACCCAACTGCTGTTTGAT
GCCGATGGCACGCTGATTCAGCGTCGCCGTAAAATCACCCCAACTCACCTGGAACGTAT
GATTTGGGGTCAGGGTGATGGTTCTGGTCTGCGTGCGGTTGATTCCGCCGTGGGCCGC
ATTGGTCAGCTGGCGTGTTTCGAACATAACAACCCACTGGCCCGTTACGCGATGATCGC
TGATGGCGAACAAATCCATTCTGCGATGTATCCGGGCAGCGCTTTTGGCGAAGGTTTTG
CGCAGTGGATGGAAATCAACATTCGTCAGCACGCACTGGAATCCGGCGCGTTCGTAGTC
AACGCAACCGCATGGCTGGATGCGGATCAGCAGGCACAAATTATGAAAGACACCGGCT
GCGGCATTGGTCCAATTAGCGGTGGTTGTTTCACCACCATTGTTTCCCCGGACGGTATG
CTGATGGCTGAACCGCTGCGCTCTGGTGAGGGCGAGGTCATCGTTGACCTGGACTTTG
CACAGATCGATCGTCGTAAAATGCTGATGGACGCTGCCGGTCATTACAACCGTCCGGAA
CTGCTGTCTCTGATGATCGATCGTACCCCTACCGCGCATGTACATGAACGTGCGCCGCA
CTCCCTGCCGGTAAGCGACAAAGCGGACGACGACGTGCGCACCCAAGCGGCTGCAGTC
GCGGGTTCCCGCCTCGAGATT